Refrigeration in 2D: Electrostaticaloric effect in monolayer materials

Daniel A. Rehn
Department of Mechanical Engineering, Stanford University, Stanford, California 94305, USA

Yao Li
Department of Applied Physics, Stanford University, Stanford, California 94305, USA

Evan J. Reed*
Department of Materials Science and Engineering, Stanford University, Stanford, California 94305, USA

(Received 3 September 2018; published 12 November 2018)

As electrical device components are scaled down to atomic sizes, management of waste heat becomes a major issue in device performance. Minimizing energy consumption of electrical components and waste heat generation are critical issues in the operation of such devices. Interest in alternative cooling mechanisms, such as those provided by electrocaloric, magnetocaloric, elastocaloric, and thermoelectric materials, may also be necessary in mitigating issues associated with waste heat generation. In this work, we provide theoretical predictions for an alternative cooling mechanism, accomplished by utilizing electrostatic gating to induce structural phase transitions in monolayer materials. We refer to this mechanism as the *electrostaticaloric* effect in reference to the mechanism of electrostatic doping that drives the structural phase transformation and entropy change in the material. Recent predictions and experimental observation that electrostatic gating can induce structural phase transformations in monolayer materials opens the possibility for new application areas. Here, we explore the potential for electrostatically induced structural phase transformations in monolayer $MoTe_2$ to be used in a Carnot refrigeration cycle. We predict that a temperature change of 10–15 K may be possible in devices that utilize monolayer $MoTe_2$ as the active phase change material. This mechanism may prove useful for future electrical devices which require cooling at the component level, and for which small monolayer devices are necessary.

DOI: 10.1103/PhysRevMaterials.2.114004

I. INTRODUCTION

Progress in transistor technology over the past several decades has led to rapid advances in computing capability in everything from industrial-scale computers to laptops and phones. As this technology matures, waste heat generated by electrical components presents fundamental limits to device miniaturization, performance, and cost [1]. For example, industrial-scale supercomputers require enormous air conditioning systems with high yearly electricity costs. The US Department of Energy reported that data centers alone accounted for 1.8% of total electricity consumed in the United States in 2014, with projected increases by 2020 [2].

The need to control waste heat generated by electrical devices has spurred research in new forms of cooling technology, including thermoelectric [3], elastocaloric [4,5], electrocaloric [6–11], and magnetocaloric [12] cooling. These cooling mechanisms require fundamentally new materials that efficiently remove waste heat from the surrounding environment. The ability to dynamically turn on cooling components via electric and/or magnetic fields could enable future devices to maintain a steady temperature profile without the need to convectively cool device components with air or fluid-based cooling systems. In addition, integration of these cooling materials at the circuit level could improve the efficiency with which waste heat is removed from electrical components.

In this work, we present our theoretical prediction that refrigeration cycles in 2D materials may be made possible by utilizing electrostatic gating to induce structural phase transformations. This effect is fundamentally distinct from electrocaloric and other cooling mechanisms, since it is the process of electrostatic doping, not electric field, that drives the structural phase transformation and entropy change in these materials. We therefore refer to this effect as the *electrostaticaloric* effect. In previous work, we demonstrated that a structural phase transition from the semiconducting $2H$ phase to the semimetallic $1T'$ phase in monolayer $MoTe_2$ can be induced via electrostatic gating [13,14]. These predictions were subsequently confirmed in experiments employing ionic liquids to gate the monolayer [15]. The $2H$ to $1T'$ phase transition in monolayer $MoTe_2$ involves an entropy change, with the entropy of the $1T'$ phase being higher than the $2H$ phase for temperatures below 1000 K (see Fig. 1 of the Supplemental Material [16]). The ability to control the phase of the monolayer via electrostatic gating and the associated entropy change between phases opens the possibility to control the temperature of the monolayer and therefore study refrigeration cycles.

*evanreed@stanford.edu

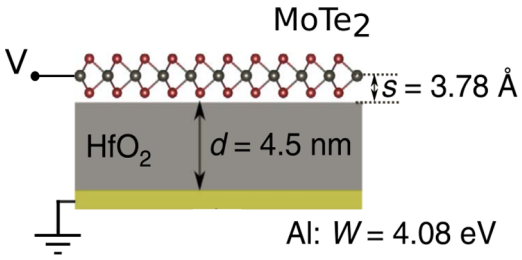

FIG. 1. Capacitor structure used to gate the monolayer. A voltage V is applied to the $MoTe_2$ monolayer, which is located a distance $s = 3.78$ Å from a dielectric. The dielectric is chosen to be HfO_2 of thickness $d = 4.5$ nm and dielectric constant $k = 25$. The dielectric sits on a grounded metal electrode, which is chosen to be aluminum with work function $W = 4.08$ eV. In this setup we assume constant zero stress on the monolayer during the phase transformation from the $2H$ to $1T'$ phase. This figure is reproduced from Ref. [14].

In this work we study the theoretical limits of Carnot refrigeration cycles in electrostatically gated monolayer $MoTe_2$. First, we present an overview of the monolayer capacitor setup used to control the temperature of the monolayer via an externally applied gate voltage and compare the refrigeration cycle in this device with the liquid-vapor Carnot refrigeration cycle. We also derive an expression for adiabats along the voltage-temperature phase boundary between the $2H$ and $1T'$ phases. Using an expression for the adiabats, we calculate the temperature change along the adiabat moving from the higher entropy $1T'$ phase to the lower entropy $2H$ phase. Additionally, we present an expression for the coefficient of performance and an estimate of the voltage and charge transfer requirements for such Carnot refrigeration cycles. Lastly, we present ideas for experiments that could be performed to measure a temperature change in monolayer $MoTe_2$.

II. THEORETICAL APPROACH

Some transition metal dichalcogenide (TMD) monolayers, including $MoTe_2$, can exist in both bulk and monolayer form. Monolayer $MoTe_2$ can exist in multiple phases with differing electronic properties. Of particular interest are the semiconducting trigonal prismatic state found in the bulk $2H$ structure and the semimetallic distorted octahedral state found in the bulk monoclinic and orthorhombic structures. The energy difference between these two phases has been calculated to be around 31 meV/f.u., lower than other Mo-based and W-based TMDs [17], making monolayer $MoTe_2$ a good candidate for phase change memory applications [14]. Structural phase transformations between these two phases in monolayer $MoTe_2$ have been predicted or reported to be driven by chemical adsorption [18], strain [17], alloying [19,20], and temperature [19,21]. More recently, electrostatic doping has been predicted [13] and reported [15] to drive a phase transition between the $2H$ and $1T'$ phases in monolayer $MoTe_2$, and the thermodynamics and energy consumed in this process have been studied [14]. In this work, we focus specifically on the electrostatic gating mechanism and how the induced structural phase transition can be used to control heat transfer to the monolayer.

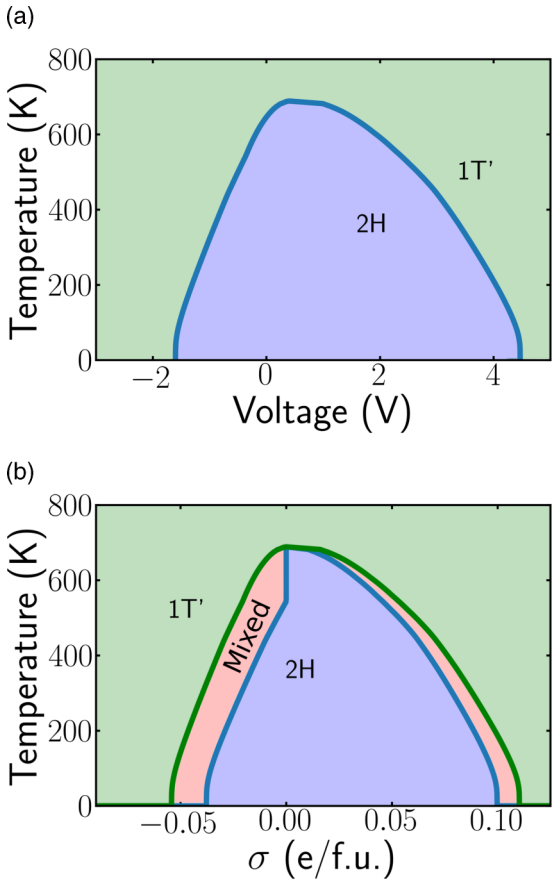

FIG. 2. Phase diagrams for electrostatically gated monolayer $MoTe_2$ in the capacitor setup shown in Fig. 1. (a) Temperature-voltage phase boundary for monolayer $MoTe_2$. Blue shading corresponds to regions where $2H$ phase is most stable, while green corresponds to regions where $1T'$ phase is most stable. (b) Temperature–excess charge phase diagram. In addition to the shadings of (a), the red shading indicates regions where a mixed $2H$ and $1T'$ phase is most stable. This figure is reproduced from Ref. [14] for clarity.

In this section, we develop both an intuitive picture and mathematical model of a Carnot refrigeration cycle for electrostatically gated monolayer $MoTe_2$. We consider gating the monolayer in the capacitor structure in Fig. 1. Details on the capacitor structure and computational approach are developed in Ref. [13] and Ref. [14]. We use the following parameters for the computational setup described in Ref. [14]: aluminum electrode of work function $W = 4.08$ eV, HfO_2 dielectric with dielectric constant $k = 25$ and thickness $d = 4.5$ nm, monolayer-dielectric distance $s = 3.78$ Å from the top of the dielectric to the Mo atom center in the monolayer, and constant zero stress throughout (i.e., the monolayer is free to relax on the dielectric without friction).

The refrigeration cycle considered here relies fundamentally on the entropy change between the $2H$ and $1T'$ phases of monolayer $MoTe_2$ and the existence of a mixed $2H$ and $1T'$ coexistence phase at the transition voltage [see Figs. 2(a) and 2(b)]. At each temperature below the predicted transition temperature of $T_m = 690$ K, two $2H$-to-$1T'$ transition voltages exist: one for positive gating and one for negative gating. The transition temperature computed using DFT-based

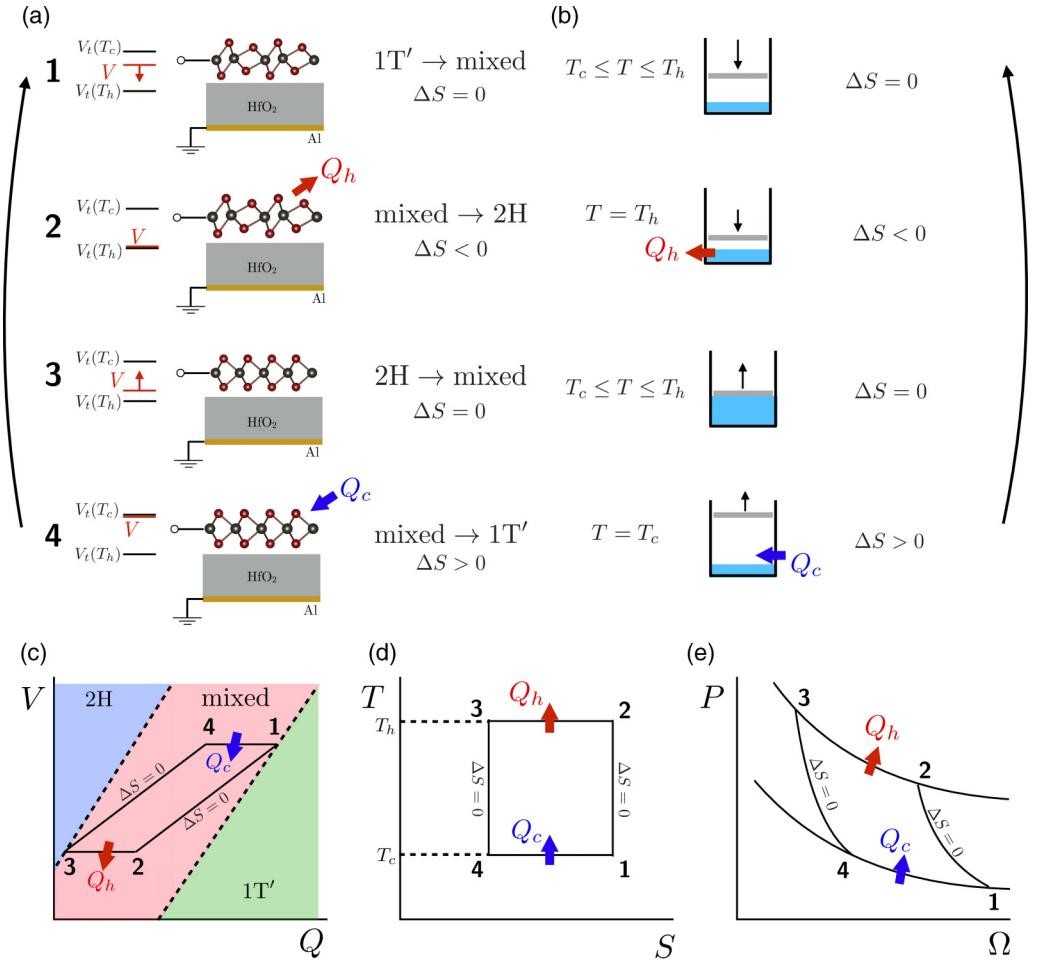

FIG. 3. Comparison of liquid-vapor refrigeration cycle and electrostatically gated monolayer $MoTe_2$ refrigeration cycle. (a) Schematic of Carnot refrigeration cycle for electrostatically gated monolayer $MoTe_2$. (b) Schematic of Carnot refrigeration cycle for the liquid-vapor case, illustrating the parallels to the electrostatic gating case. (c) Schematic of Carnot refrigeration cycle for monolayer $MoTe_2$ in voltage-charge (V-Q) space. (d) Temperature-entropy (T-S) cycle for both monolayer $MoTe_2$ and the liquid-vapor case. Phase boundaries are not shown because the phase boundaries are different for the monolayer $MoTe_2$ and liquid-vapor cases; however, the vertical and horizontal lines occur in both cases. (e) Pressure-volume (P-Ω) refrigeration cycle for the liquid-vapor case.

calculations at zero excess charge is lower than experimental numbers for bulk $MoTe_2$ near 1100 K [22]. This discrepancy has been reported previously when including spin-orbit coupling (SOC) corrections in DFT calculations [19], leading to a transition temperature of around 640 K with inclusion of SOC effects and above 900 K without inclusion of SOC effects. Our calculations include SOC effects and predict a transition temperature in good agreement with Ref. [19] using a fundamentally different method to compute the transition temperature [14]. In this work, we focus on positive gating and therefore can consider the transition voltage to be in one-to-one correspondence with temperature in the range $V > 0$ V and $0 \leqslant T < T_m$ [see Fig. 2(a)]. This allows us to consider processes in which we directly control the temperature of the monolayer by changing the externally applied voltage.

An intuitive picture of the refrigeration cycle can be made by comparing the Carnot refrigeration cycle of a liquid-vapor phase to the electrostatically gated monolayer $MoTe_2$ cycle, shown in Fig. 3. In the liquid-vapor case of Fig. 3(b), we consider applying pressure to a cylinder and changing the volume Ω of the cylinder. Starting at the top of Fig. 3(b), we consider isentropic (and adiabatic) compression, in which we compress the cylinder, decreasing the volume of the system. During this process the temperature of the system begins at T_c and ends at a higher temperature T_h. The next step is condensation, in which the vapor in the cylinder is allowed to exchange heat with an external reservoir. In this process, the temperature is held constant at $T = T_h$, so that an amount of heat Q_h leaves the vapor, causing a transformation to a liquid state. The next step is isentropic expansion, in which the cylinder expands adiabatically and isentropically, changing the temperature of the liquid from T_h to T_c, and therefore causing the system to enter a mixed liquid-vapor state. The last step is evaporation, in which the system is held at T_c and allowed to exchange heat with the surroundings. In this case, an amount of heat Q_c flows into the system and some of the liquid is transformed to vapor. These steps are illustrated schematically in Figs. 3(d) and 3(e). Figure 3(d) shows the cycle in terms of temperature and entropy, while Fig. 3(e) shows the cycle in terms of pressure and volume (Ω). Notably, the temperature-entropy case in Fig. 3(d) is qualitatively the

same in both the liquid-vapor case and electrostatically gated monolayer $MoTe_2$ case.

As with the liquid-vapor case, the Carnot refrigeration cycle for electrostatically gated monolayer $MoTe_2$ consists of two adiabatic steps and two isothermal steps, as shown in Fig. 3(a). Because of the one-to-one correspondence between temperature and transition voltage [see Fig. 2(a)], the electrostatic gating cycle also consists of two constant voltage steps, which occur simultaneously with the isothermal steps. Starting at the top of the figure, we consider beginning in the $1T'$ phase at temperature T_c and maximum voltage $V_t(T_c)$. We then adiabatically reduce the voltage to $V_t(T_h)$. As shown in Fig. 2, a lower transition voltage corresponds to a higher transition temperature, and therefore this process ends at a higher temperature, T_h. During this process, the monolayer starts in the $1T'$ phase and ends at a mixed $1T'$ and $2H$ phase. The degree of the mixing depends on the ending transition voltage, as described later. In the next step, the monolayer is held at a fixed temperature T_h and voltage $V_t(T_h)$ as heat Q_h leaves the monolayer. In this process, charge is removed from the monolayer, moving from the mixed $2H$ and $1T'$ coexistence phase to an entirely $2H$ phase. Next, the voltage is increased from $V_t(T_h)$ to $V_t(T_c)$ and the monolayer adiabatically transforms from entirely $2H$ to a mixed $2H$ and $1T'$ phase. During this process, the temperature decreases from T_h to T_c. Lastly, the monolayer is held at fixed voltage $V_t(T_c)$ and temperature T_c while heat Q_c enters the monolayer. A schematic of the refrigeration cycle in terms of voltage and charge is shown in Fig. 3(c). Additionally, the cycle for monolayer $MoTe_2$ in terms of temperature and entropy is shown in Fig. 3(d), which is qualitatively the same as the liquid-vapor case.

To construct a mathematical model of the refrigeration cycle for electrostatically gated monolayer $MoTe_2$, an expression for the adiabats in the mixed phase region is needed. For this, we begin by writing down the total entropy of the monolayer in terms of the temperature T and fraction of $2H$ present, x. We assume linear mixing with $x = 0$ corresponding to the entirely $1T'$ phase and $x = 1$ corresponds to the entirely $2H$ phase. With the assumption of linear mixing, we write the total entropy along the $2H$-$1T'$ phase boundary as

$$S(T, x) = xS_{2H}(T) + (1 - x)S_{1T'}(T). \tag{1}$$

Within the mixed phase, we look for constant entropy contours, so that

$$0 = dS = \left(\frac{\partial S}{\partial T}\right)_x dT + \left(\frac{\partial S}{\partial x}\right)_T dx, \tag{2}$$

where the subscripts refer to variables held constant during partial differentiation. Here we take the material to be at a state of constant zero stress. Evaluating and rearranging leads to

$$\frac{dT}{dx} = T\frac{S_{1T'}(T) - S_{2H}(T)}{xC_{2H} + (1 - x)C_{1T'}}, \tag{3}$$

where the partial derivatives with respect to T have been rewritten in terms of the heat capacity,

$$\frac{\partial S}{\partial T} = \frac{C_x(T)}{T}, \tag{4}$$

where C_x is the heat capacity at a given phase fraction x. The entropy and heat capacity consist of both electronic and vibrational (phonon) contributions, i.e., $S = S^{\text{el}} + S^{\text{ph}}$ and $C = C^{\text{el}} + C^{\text{ph}}$. DFT calculations show that the electronic contribution to the heat capacities of the $2H$ and $1T'$ phases is around 1% of the vibrational contribution to the heat capacity. We therefore neglect the term C^{el}, so that $C = C^{\text{ph}}$. In addition, the vibrational heat capacities of the $2H$ and $1T'$ phases vary individually by at most 0.8% in the temperature range we consider for refrigeration cycles, $T = 270$ K to $T = 290$ K (see Fig. 2 of the Supplemental Material [16]). For our purposes, we approximate the heat capacity of the $2H$ and $1T'$ phases separately as constants within this range of temperatures using the computed values at $T = 280$ K as the constant values, which are $C_{2H} = 1.53\ \text{J K}^{-1}\ \text{cm}^{-3}$ and $C_{1T'} = 1.54\ \text{J K}^{-1}\ \text{cm}^{-3}$. We may also define $\Delta C \equiv C_{1T'} - C_{2H}$. ΔC is less than 1% of $C_{1T'}$, so we ignore the term $x\Delta C$ in the denominator of Eq. (3). In addition, DFT calculations show that the entropy difference $\Delta S(T) = S_{1T'}(T) - S_{2H}(T)$ varies by only 1% in the same temperature range $270\ \text{K} \leqslant T \leqslant 290\ \text{K}$. Therefore, we neglect the temperature dependence and instead define $\Delta S \equiv \Delta S(280\ \text{K})$ to be used in the integration. Using these approximations, we integrate Eq. (3) as

$$\int_{T_i}^{T_f} \frac{dT}{T\Delta S} = \int_{x_i}^{x_f} \frac{dx}{C_{1T'}}, \tag{5}$$

where T_i (x_i) and T_f (x_f) are the initial and final temperatures ($2H$ fractions), respectively. Upon integrating, the final temperature T_f can be solved in terms of T_i, x_i, and x_f,

$$T_f = T_i \exp\left\{(x_f - x_i)\frac{\Delta S}{C_{1T'}}\right\}. \tag{6}$$

Equation (6) provides an expression for the final temperature of the monolayer in terms of the initial and final $2H$ fractions. Due to the one-to-one correspondence of temperature and voltage $T(V)$ for $V > 0$, as well as the correspondence of x with the excess charge Q on the monolayer $x(Q)$, it is possible to plot the trajectory of the Carnot refrigeration cycle in terms of T-x space and V-Q space. We consider both perspectives below. These perspectives refer to the same cycle, but help to identify the change in temperature or voltage/excess charge that occurs during a single cycle. Lastly, we point out that one common measure of performance for refrigeration cycles is the coefficient of performance (COP), defined as the ratio of the amount of heat transferred from the cold reservoir to the monolayer Ξ_c to the amount of work done in one cycle W,

$$\text{COP} = \frac{\Xi_c}{W}. \tag{7}$$

In the case of a Carnot cycle, the first law of thermodynamics states that $\Xi_h = \Xi_c + W$ where Ξ_h is the waste heat dumped to the surroundings. In this case, $\text{COP} = \Xi_c/(\Xi_h - \Xi_c)$. For a liquid-vapor phase, the entropy change of the liquid/vapor phase at the high and low temperatures is the same, which allows us to write the COP in terms of the high and low temperatures alone. For monolayer $MoTe_2$, we approximate the entropy change at the high and low temperatures as equal, as discussed previously. Therefore, it is possible to write the COP in terms of the high and low temperatures (T_i and T_f)

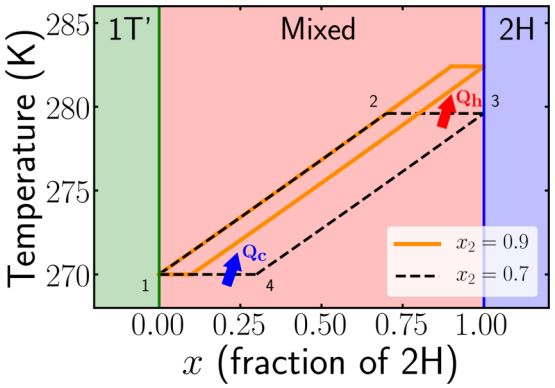

FIG. 4. Refrigeration cycle in T-x space for two different values $x_2 = 0.7$ and $x_2 = 0.9$. The numbers on the plot correspond to the steps outlined in Fig. 3(a). Regions where $1T'$ is most stable are shown in the green shaded region, regions where $2H$ is most stable are shown in the blue shaded region, and regions where a mixed $2H$ and $1T'$ phase is most stable are shown in the red shaded region.

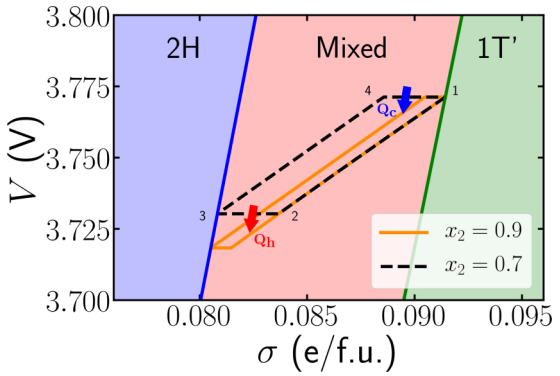

FIG. 5. Carnot refrigeration cycle in voltage–excess charge space (excess charge per formula unit σ is plotted on the x axis). The cycle takes place entirely within the red shaded region, where a mixed $2H$ and $1T'$ coexistence phase is most stable. The blue shaded region indicates regions where the $2H$ phase is most stable, and the green shaded region corresponds to regions where the $1T'$ phase is most stable. The material is moved around the circuit through control of the excess charge σ.

by taking $\Xi_c = T_i \Delta S$ and $\Xi_h = T_f \Delta S$. The COP can then be written as $\mathrm{COP} = 1/(T_f/T_i - 1)$. Using Eq. (6), the COP becomes

$$\mathrm{COP} = \frac{1}{\exp\left\{(x_f - x_i)\frac{\Delta S}{C_{1T'}}\right\} - 1}. \tag{8}$$

Additional details on the COP and a plot of the COP for monolayer $MoTe_2$ are included in the Supplemental Material [16]. We find that for a full transition from the $1T'$ to $2H$ phase, $\mathrm{COP} = 19$ corresponding to a temperature change from 270 K to 284 K. This value for the COP provides an upper bound to COP values that could be measured in the laboratory. Experimentally reported values of the COP for elastocaloric and magnetocaloric materials in the operating range of 288–298 K have been reported between 50%–90% of the Carnot limit $\mathrm{COP} = 29$ [23]. Because the electrostaticaloric cooling mechanism presented here is new, experimental values of the COP are not yet known.

III. RESULTS

Here, we present results for a refrigeration cycle that follows the steps outlined in Fig. 3(a). We consider starting in the $1T'$ phase at $T = 270$ K. Since there are four distinct paths in this cycle, it is most convenient to label the $2H$ fractions and temperatures according to the numbered stages in Fig. 3, rather than label them as x_i, x_f, as described previously. The initial point of entirely $1T'$ phase will therefore be $x_1 = 0$, $T_1 = 270$, followed by x_2, T_2, and so on. The values in V-Q space will also be labeled by the same subscripting convention.

Note that once x_1 and T_1 are specified, temperature T_2 is determined by specification of the $2H$ fraction present at the end of the adiabat, x_2. After specifying x_2, the rest of the cycle is uniquely determined if we assume that a complete transformation to the $2H$ phase and subsequently $1T'$ phase occurs, and that the cycle returns to T_1 and repeats.

In Fig. 4, we show the refrigeration cycle in T-x space for two different values, $x_2 = 0.7$ and $x_2 = 0.9$. In the figure, the green shading corresponds to regions where $1T'$ is most stable, the blue shading corresponds to regions where $2H$ is most stable, and red shading corresponds to regions where a mixed $2H$ and $1T'$ phase is most stable.

Figure 4 shows that the larger value of x_2 gives rise to a larger temperature change in the monolayer, as expected. In this Carnot limit, we predict it would be possible to change the temperature of the monolayer by 10–15 K.

In Fig. 5, we show the same refrigeration cycle in V-Q space (note that instead of excess charge Q, the excess charge per formula unit σ is plotted). Figure 5 illustrates how the cycle can be controlled via electrostatic gating. Shaded regions in the figure correspond to regions of stability, as in Fig. 4. Control of the charge σ drives the state of the material around the circuit, acting like the volume of the piston Ω in Fig. 3.

Figure 5 also illustrates how the temperature of monolayer $MoTe_2$ can be controlled via voltage. The paths from point 1 to point 2 and from point 3 to point 4 are the adiabats, where no heat transfer to or from the monolayer occurs and the entropy remains constant. During these processes, the temperature of the monolayer increases (point 1 to 2) or decreases (point 3 to 4) accordingly. The magnitude of temperature change is determined by Eq. (6), while the magnitude of the change in voltage required is determined by the computed temperature-voltage phase diagram shown in Fig. 2(a).

These phase diagrams are computed with the assumption that the $2H$ to $1T'$ phase transition takes place under constant zero stress. This means that the lattice may relax freely on the substrate with no friction, if a substrate is employed. For cases in which the friction on an employed substrate is non-negligible, a more appropriate thermodynamic constraint could be that of a fixed lattice. We studied the fixed lattice case in Ref. [13] and found that the amount of excess charge needed to drive the $2H$ to $1T'$ phase transition is approximately double that needed in the constant zero stress case. In both the fixed lattice and constant zero stress cases, the underlying physics is expected to be qualitatively similar so

that refrigeration cycles will differ only quantitatively from those in Figs. 4 and 5.

The Carnot refrigeration cycle for electrostatically gated monolayer $MoTe_2$ will require careful attention to the kinetics of the phase transformation from the $2H$ to $1T'$ phase at different points in the cycle. For the isentropic portions of the cycle, the transition needs to happen fast enough that no heat enters or escapes the monolayer, yet sufficiently slow that the transformation is isentropic. In addition, constant temperature portions of the cycle must be slow enough to allow the kinetics of mixed phase evolution to be at equilibrium. A lower bound on the amount of time required during these stages can be set by the rate of the transformation from a mixed $2H+1T'$ phase to either the $2H$ or $1T'$ phase, depending on the stage in the cycle. Experimental studies of the kinetics of the transition in monolayer $MoTe_2$ are still sparse, with studies reporting a transition time ranging from less than minutes [15,24] to hours [21,25]. Further investigations may help to shed light onto the appropriate timescales for controlling the charge transfer to the monolayer during the refrigeration cycle. We discuss the role of kinetics and hysteresis in devices in detail in the Supplemental Material [16].

While the electrostaticaloric effect presented here has been illustrated quantitatively by way of $MoTe_2$, it is expected to be applicable to a much broader spectrum of thin materials. Here we ask what other materials might serve as better phase change refrigeration devices. Perhaps most importantly, the ideal material should have fast kinetics for quickly transitioning from one phase to another. Materials with fast kinetics can potentially be cycled very quickly, to allow for greater efficiency in removing heat from their surroundings. In addition, the best materials for refrigeration applications have large latent heats [23], owing to the fact that this allows for a large transfer of heat during the phase transition and a large mixed phase region in charge in which the device can operate. Ideal materials would also have relatively low heat capacity, so that the energy input required to change the temperature of the material is small compared to the latent heat of the transformation. The transitions do not necessarily need to be structural in nature. For example, electronic transitions such as charge density wave transitions with high latent heat could potentially be employed. In addition, monolayer materials with large changes in phonon frequencies upon electrostatic gating may yield entropy changes sufficiently large to be useful.

Lastly, we propose two general ideas for measuring the temperature change experimentally. While the kinetics of the phase change in $MoTe_2$ are relatively unknown, they may be sufficiently slow that the condition of adiabaticity will be challenging to maintain for a single layer on a substrate. Therefore, indirect approaches involving isothermal measurements may be easier. Following the work of Mischenko *et al.* [26] in measuring the temperature change of the electrocaloric material $PbZr_{0.95}Ti_{0.05}O_3$, we propose the following experiment to perform with monolayer $MoTe_2$:

(1) Under isothermal conditions, gate the monolayer in the setup of Fig. 1, starting from 0 V and increasing through the transition voltage, then back to 0 volts (inducing the transition with negative values of voltage is also possible). During the gating process, measure the excess charge Q transferred to the monolayer using, e.g., the Hall current to back out the charge supplied to the monolayer, as discussed in Ref. [15]. Doing so should provide a set of measurements (V, Q) in one cycle of the voltage.

(2) Repeat the measurement done in step 1 over a range of (fixed) temperatures. Each temperature measurement should provide a unique hysteresis loop of (V, Q), similar to the (E, P) measurements taken in Ref. [26] (where $E =$ electric field and $P =$ polarization in the material).

(3) Using the data in steps 1, 2, compute $Q(T; V)$, the excess charge as a function of temperature and for V fixed across the different temperature measurements. Doing so will essentially map out the excess charge vs temperature phase diagram presented in Fig. 2(b). This can be done for a range of fixed voltages V.

(4) Compute the temperature change using the following thermodynamic relationship for an adiabatic temperature change (see the Supplemental Material [16] for a derivation),

$$\Delta T = -\int_{V_1}^{V_2} \frac{T}{C_V}\left(\frac{\partial Q}{\partial T}\right)_V dV, \tag{9}$$

where C_V is the heat capacity at constant voltage, V_1 is the voltage associated with the lowest temperature measurement, and V_2 is another (higher) voltage. As shown in Fig. 2 of the Supplemental Material [16], the heat capacity for $MoTe_2$ is roughly constant above 250 K and is approximately the same for the $2H$ and $1T'$ phases, so that estimating C_V as a constant should be acceptable in Eq. (9).

The series of isothermal measurements of (V, Q), along with the expression for the temperature change in Eq. (9), can be viewed as an indirect way of measuring the total temperature change of the monolayer.

An alternative second approach to measuring the temperature change in the monolayer would involve a direct measurement of the temperature change using a surface probe on the monolayer as the monolayer changes phase from $2H$ to $1T'$. It may be possible to measure a temperature change from the Raman spectrum using the peak frequency shifts as a measure of the temperature change. It may also be possible to use scanning thermal microscopy on the top of the monolayer to measure a temperature change directly as charge is added. In this setup, it would be necessary to gate the monolayer via an ionic liquid placed underneath the monolayer, rather than on top of the monolayer, as was done in Ref. [15].

The two approaches to experiments mentioned above may help to provide a measurement of the temperature change in $MoTe_2$ across the transition from $2H$ to $1T'$, and may also help to elucidate the nature of the excess charge vs temperature phase boundary, which is shown in Fig. 2(b).

IV. CONCLUSIONS

In this work we presented theoretical predictions that monolayer materials that undergo structural phase transitions driven by electrostatic gating may be utilized to absorb heat and act as two-dimensional refrigeration devices. The mechanism allowing for heat to be absorbed is distinct from electrocaloric and other cooling mechanisms, and we therefore refer to this mechanism as the *electrostaticaloric* effect. We predict that for monolayer $MoTe_2$-based devices, temperature

changes of 10–15 K can occur along the adiabatic transformation from the $1T'$ or $2H$ phases to a mixed $2H+1T'$ phase, with the precise value of temperature change depending on the degree of transformation. We predict that the temperature change can be controlled directly via an applied gate voltage under adiabatic conditions, providing an externally tunable mechanism for adjusting the temperature. Furthermore, we have outlined possible experiments that could be performed to measure a temperature change in the monolayer.

Devices that utilize this effect could potentially be useful for future electronic devices that require cooling capability at the component level, since 2D materials have the potential to be integrated deep into electronic devices. An interesting possibility is to combine this cooling capability with phase change memory devices [14]. Generally, incorporating active cooling capability at the component level may allow for future devices to retain a steady operating temperature profile at higher device densities without the need for conductive or convective cooling, as is employed in current devices.

V. METHODS

All periodic DFT calculations were performed with the Vienna *Ab initio* Simulation Package (VASP) [27], version 5.3.3 and/or 5.3.5. The calculations use the projector augmented-wave [28,29] method and the electron exchange-correlation interaction was treated by the generalized gradient approximation (GGA) functional of Perdew, Burke, and Ernzerhof (PBE) [30]. A kinetic energy cutoff of 350 eV for the plane-wave basis set was used for all electrostatic gating calculations. All atomic structures and in-plane lattice constants were relaxed using the conjugate gradient algorithm. The convergence thresholds for ionic and electronic relaxations were 10^{-7} eV and 10^{-8} eV, respectively. A 2 f.u. unit cell with an $18\times18\times1$ Monkhorst-Pack [31] **k**-point mesh for the Brillouin zone sampling was employed for the calculations done in Figs. 4 and 5. These figures also used a 36 Å **c** axis to introduce vacuum space (perpendicular to the plane of the monolayer) to prevent interaction between periodic cell repeats, as well as a Gaussian electronic energy distribution smearing of 50 meV to aid in energy convergence. These calculations also included noncollinear spin-orbit coupling. The electronic entropies of $2H$ and $1T'$ phases of $MoTe_2$ were computed directly from VASP using Fermi-Dirac smearing with spin-orbit coupling. The vibrational (phonon) entropies of $2H$- and $1T'$-$MoTe_2$ were computed from the phonon density of states using the Phonopy [32] Python package. These phonon calculations used VASP's built-in density functional perturbation theory method (IBRION=8) and a $2\times2\times1$ (8 f.u.) supercell generated from the relaxed lattice positions of the 2 f.u. unit cell used in Figs. 4 and 5. The supercell uses a **c** axis of 16 Å (along the direction perpendicular to the layer) and an $18\times18\times1$ Monkhorst-Pack **k**-point mesh. These simulations also included noncollinear spin-orbit coupling, with an electronic relaxation threshold of 10^{-5} eV.

All data used to generate the results and figures in this paper are available [33].

ACKNOWLEDGMENTS

We thank A. Salleo, D. Zakhidov, and E. Pop for useful discussions regarding topics discussed above. This work was partially supported by NSF Grants No. EECS-1436626 and No. DMR-1455050, Army Research Office Grant No. W911NF-15-1-0570, Office of Naval Research Grant No. N00014-15-1-2697, and a seed grant from Stanford System X Alliance. This work was supported in part by the US Army Research Laboratory, through the Army High Performance Computing Research Center, Cooperative Agreement No. W911NF-07-0027.

[1] S. Krishnan, S. V. Garimella, G. M. Chrysler, and R. V. Mahajan, Towards a thermal Moore's law, in *ASME 2005 Pacific Rim Technical Conference and Exhibition on Integration and Packaging of MEMS, NEMS, and Electronic Systems collocated with the ASME 2005 Heat Transfer Summer Conference* (American Society of Mechanical Engineers, Berkeley, California, 2005), pp. 591–603.

[2] A. Shehabi, S. Smith, D. Sartor, R. Brown, M. Herrlin, J. Koomey, E. Masanet, N. Horner, I. Azevedo, and W. Lintner, United States Data Center Energy Usage Report (2016).

[3] X. Zhang and L.-D. Zhao, Thermoelectric materials: Energy conversion between heat and electricity, J. Materiomics **1**, 92 (2015).

[4] S. Qian, Y. Geng, Y. Wang, J. Ling, Y. Hwang, R. Radermacher, I. Takeuchi, and J. Cui, A review of elastocaloric cooling: Materials, cycles, and system integrations, Int. J. Refrig. **64**, 1 (2016).

[5] J. Tušek, K. Engelbrecht, R. Millán-Solsona, L. Mañosa, E. Vives, L. P. Mikkelsen, and N. Pryds, The elastocaloric effect: A way to cool efficiently, Adv. Energy Mater. **5**, 1500361 (2015).

[6] S.-G. Lu, Q. M. Zhang, and Z. Kutnjak, The electrocaloric effect (ECE) in ferroelectric polymer films, in *Thin Film Growth* (Elsevier, Cambridge, UK, 2011), pp. 364–383.

[7] Z. Kutnjak, B. Rožič, and R. Pirc, Electrocaloric effect: Theory, measurements, and applications, Wiley Encyclop. Electr. Electron. Eng., 1 (1999), doi:10.1002/047134608X.W8244.

[8] M. Valant, Electrocaloric materials for future solid-state refrigeration technologies, Prog. Mater. Sci. **57**, 980 (2012).

[9] S.-G. Lu and Q. Zhang, Electrocaloric materials for solid-state refrigeration, Adv. Mater. **21**, 1983 (2009).

[10] C. Aprea, A. Greco, A. Maiorino, and C. Masselli, Electrocaloric refrigeration: An innovative, emerging, eco-friendly refrigeration technique, J. Phys.: Conf. Ser. **796**, 012019 (2017).

[11] M. Ožbolt, A. Kitanovski, J. Tušek, and A. Poredoš, Electrocaloric refrigeration: Thermodynamics, state of the art, and future perspectives, Int. J. Refrig. **40**, 174 (2014).

[12] J. R. Gómez, R. F. Garcia, A. De Miguel Catoira, and M. R. Gómez, Magnetocaloric effect: A review of the thermodynamic cycles in magnetic refrigeration, Renew. Sustain. Energy Rev. **17**, 74 (2013).

[13] Y. Li, K.-A. N. Duerloo, K. Wauson, and E. J. Reed, Structural semiconductor-to-semimetal phase transition in two-dimensional materials induced by electrostatic gating, Nat. Commun. **7**, 10671 (2016).

[14] D. A. Rehn, Y. Li, E. Pop, and E. J. Reed, Theoretical potential for low energy consumption phase change memory utilizing electrostatically-induced structural phase transitions in 2D materials, npj Comput. Mater. **4**, 2 (2018).

[15] Y. Wang, J. Xiao, H. Zhu, Y. Li, Y. Alsaid, K. Y. Fong, Y. Zhou, S. Wang, W. Shi, Y. Wang, A. Zettl, E. J. Reed, and X. Zhang, Structural phase transition in monolayer $MoTe_2$ driven by electrostatic doping, Nature (London) **550**, 487 (2017).

[16] See Supplemental Material at http://link.aps.org/supplemental/10.1103/PhysRevMaterials.2.114004 for additional derivations and density functional theory based calculations.

[17] K.-A. N. Duerloo, Y. Li, and E. J. Reed, Structural phase transitions in two-dimensional Mo- and W-dichalcogenide monolayers, Nat. Commun. **5**, 4214 (2014).

[18] Y. Zhou and E. J. Reed, Structural phase stability control of monolayer $MoTe_2$ with adsorbed atoms and molecules, J. Phys. Chem. C **119**, 21674 (2015).

[19] K.-A. N. Duerloo and E. J. Reed, Structural phase transitions by design in monolayer alloys, ACS Nano **10**, 289 (2015).

[20] D. Rhodes, D. A. Chenet, B. E. Janicek, C. Nyby, Y. Lin, W. Jin, D. Edelberg, E. Mannebach, N. Finney, A. Antony, T. Schiros, T. Klarr, A. Mazzoni, M. Chin, Y. C. Chiu, W. Zheng, Q. R. Zhang, F. Ernst, J. I. Dadap, X. Tong, J. Ma, R. Lou, S. Wang, T. Qian, H. Ding, R. M. Osgood Jr., D. W. Paley, A. M. Lindenberg, P. Y. Huang, A. N. Pasupathy, M. Dubey, J. Hone, and L. Balicas, Engineering the structural and electronic phases of $MoTe_2$ through W substitution, Nano Lett. **17**, 1616 (2017).

[21] T. A. Empante, Y. Zhou, V. Klee, A. E. Nguyen, I.-H. Lu, M. D. Valentin, S. A. Naghibi Alvillar, E. Preciado, A. J. Berges, C. S. Merida, M. Gomez, S. Bobek, M. Isarraraz, E. J. Reed, and L. Bartels, Chemical vapor deposition growth of few-layer $MoTe_2$ in the $2H$, $1T'$, and $1T$ phases: Tunable properties of $MoTe_2$ films, ACS Nano **11**, 900 (2017).

[22] M. B. Vellinga, R. De Jonge, and C. Haas, Semiconductor to metal transition in $MoTe_2$, J. Solid State Chem. **2**, 299 (1970).

[23] I. Takeuchi and K. Sandeman, Solid-state cooling with caloric materials, Phys. Today **68**, 48 (2015).

[24] S. Song, D. H. Keum, S. Cho, D. Perello, Y. Kim, and Y. H. Lee, Room temperature semiconductor-metal transition of $MoTe_2$ thin films engineered by strain, Nano Lett. **16**, 188 (2015).

[25] S. M. Oliver, R. Beams, S. Krylyuk, I. Kalish, A. K. Singh, A. Bruma, F. Tavazza, J. Joshi, I. R. Stone, S. J. Stranick, A. V. Davydov, and P. M. Vora, The structural phases and vibrational properties of $Mo_{1-x}W_xTe_2$ alloys, 2D Mater. **4**, 045008 (2017).

[26] A. S. Mischenko, Q. Zhang, J. F. Scott, R. W. Whatmore, and N. D. Mathur, Giant electrocaloric effect in thin-film $PbZr_{0.95}Ti_{0.05}O_3$, Science **311**, 1270 (2006).

[27] G. Kresse and J. Furthmüller, Efficient iterative schemes for *ab initio* total-energy calculations using a plane-wave basis set, Phys. Rev. B **54**, 11169 (1996).

[28] P. E. Blöchl, Projector augmented-wave method, Phys. Rev. B **50**, 17953 (1994).

[29] G. Kresse and D. Joubert, From ultrasoft pseudopotentials to the projector augmented-wave method, Phys. Rev. B **59**, 1758 (1999).

[30] J. P. Perdew, K. Burke, and M. Ernzerhof, Generalized Gradient Approximation Made Simple, Phys. Rev. Lett. **77**, 3865 (1996).

[31] H. J. Monkhorst and J. D. Pack, Special points for Brillouin-zone integrations, Phys. Rev. B **13**, 5188 (1976).

[32] A. Togo and I. Tanaka, First principles phonon calculations in materials science, Scr. Mater. **108**, 1 (2015).

[33] See https://github.com/rehnd/MoTe2Refrigeration.